

# On the Swelling of Polymer Network Strands

Michael Lang\* and Reinhard Scholz

Large scale computer simulations are employed to analyze the conformations of network strands in polymer networks at preparation conditions (characterized by a polymer volume fraction of  $\phi_0$ ) and when swollen to equilibrium (characterized by a polymer volume fraction  $\phi < \phi_0$ ). Network strands in end-linked model networks are weakly stretched and partially swollen at preparation conditions as compared to linear polymers in the same solvent at  $\phi_0$ . Equilibrium swelling causes non-ideal chain conformations characterized by an effective scaling exponent approaching 7/10 on intermediate length scales for increasing overlap of the chains. The chain size in a network consists of a fluctuating and a time average “elastic” contribution. The elastic contribution swells essentially affinely  $\propto (\phi_0/\phi)^{2/3}$ , whereas the swelling of the fluctuating part lies between the expected swelling of the entanglement constraints and the swelling of non-cross-linked chains in a comparable semi-dilute solution. The total swelling of chain size results from the changes of both fluctuating and non-fluctuating contributions.

## 1. Introduction

Polymer networks and gels are frequently used in our every day life in materials like contact lenses,<sup>[1]</sup> gelatine,<sup>[2]</sup> car tyres,<sup>[3]</sup> or diapers,<sup>[4]</sup> to provide just some examples. Despite of this broad range of applications, we understand only little of how they function. A modeling of these complex materials starts with a massive simplification of the problem: instead of considering zillions of overlapping and entangled molecules glued together randomly to a chunk of material, we boil down the problem to considering only a single chain subject to some representative interactions entering at the chain ends (like external deformation or the connections to the surrounding network) or along the chain contour (like entanglements and interactions with the surrounding chains).<sup>[5]</sup> Afterwards, we consider an isotropic ensemble of identical chains with the hope that this procedure results in reliable predictions on the macroscopic scale.

M. Lang, R. Scholz  
 Leibniz Institute of Polymer Research Dresden  
 Hohe Straße 6, 01069 Dresden, Germany  
 E-mail: [lang@ipfdd.de](mailto:lang@ipfdd.de)

 The ORCID identification number(s) for the author(s) of this article can be found under <https://doi.org/10.1002/marc.202400025>

© 2024 The Authors. Macromolecular Rapid Communications published by Wiley-VCH GmbH. This is an open access article under the terms of the [Creative Commons Attribution](https://creativecommons.org/licenses/by/4.0/) License, which permits use, distribution and reproduction in any medium, provided the original work is properly cited.

DOI: 10.1002/marc.202400025

Along this line of arguments, we rely strongly on assumptions regarding the properties of the individual chains. Up to recently, the accepted point of view concerning the equilibrium conformation of a polymer chain in a network was that it resembles the chain conformation in a polymer solution at the same polymer concentration.<sup>[6]</sup> This was first challenged by computer simulations where the time average size of the network strands was related to the embedding of these strands into the surrounding network structure:<sup>[7]</sup> elastic strands establishing short cyclic structures in the network turned out to remain more compact than those participating only in large cyclic structures. Furthermore, assembling chains together at cross-links leads to additional bond–bond correlations<sup>[8,9]</sup> which are not screened in a

melt or in a network. The resulting swelling of the chain conformations in the network causes additional deviations from the conformations of linear chains in a polymer solution,<sup>[10]</sup> renormalizing the equilibrium strand size in the network. In effect, this process may even lead to slightly deswollen average chain conformations at preparation conditions, although no solvent is removed from the reaction bath. Moreover, it was proposed that toward the final stage of e.g., an end-linking process, the chains must stretch in order to access the remaining reactive sites at the cross-links.<sup>[11]</sup> On top of this, loop closure leads to a frustrated system where adjusting the equilibrium loop size for one loop may stretch the surrounding chains.<sup>[7]</sup> Since these corrections are related to the cross-linking process, we expect a different degree of enlargement of the chain conformations depending both on the polymer architecture prior to the cross-linking and on the process of network formation.

Very recently,<sup>[12]</sup> it was shown by scattering experiments in the low concentration limit that elastic network strands should be larger than in solution by 2–23% when considering the impact of pending loops for end-linked model networks. Such corrections were not known from older work where networks were prepared at large overlap numbers: a topology blind average over pending loops and elastic chains did not show significant changes in the size of the chains upon cross-linking.<sup>[13,14]</sup> Such a comparison is bedeviled by the substantial error of the old data appearing to be larger than the measurable effect, see Figure 4 of ref. [12]. The simulation data in the literature remains inconclusive due to volume changes or when a large capture radius is assumed in the cross-linking procedure.<sup>[15,16]</sup> Therefore, to date it is not clear to which extent the conformations of the network chains comply with those in a solution at preparation conditions.

The situation becomes even more complex when the networks swell to equilibrium. To date, the Flory-Rehner hypothesis<sup>[17]</sup> forms the basis of our understanding: the osmotic pressure is counterbalanced by the elastic “pressure” of the network. In the language of the blob model, this means that the network must have as many tension blobs as correlation volumes, since any of these contributes  $\approx kT$  to either modulus or osmotic pressure of the system.<sup>[6,18]</sup> However, in several experiments and simulations on the arrested swelling of entangled globules or the swelling of networks,<sup>[19–21]</sup> it was observed that the effective exponent describing the conformations of the network chains is close to  $\nu \approx 0.7$  or even larger. This challenges the blob picture assuming chain conformations to follow the statistics of non-cross-linked chains in the corresponding solution. Several attempts to explain this behavior<sup>[19,22,23]</sup> used a scaling hypothesis, which was criticized later.<sup>[18]</sup> Older work suggested an exponent of  $\nu \approx 5/8$ <sup>[24]</sup> based upon an analogy with diluted percolation clusters and supported by scattering measurements in agreement with  $\nu \approx 2/3$ . More recently, a cross-over was proposed, interpolating from excluded volume scaling below blob size to a stretched linear arrangement of blobs up to the affine length scale of the deformations.<sup>[18]</sup> This would lead to a short range scaling  $R \propto N^{0.6}$  followed by  $R \propto N$  that might appear as an intermediate exponent close to 0.7 or similar on length scales just above the size of a correlation volume. However, the available data on the swelling of individual network strands is still quite limited<sup>[12–14,21,25–27]</sup> and suffers from the accuracy of the employed methods where rather small changes in the exponent  $\nu$  and the chain size are difficult to track.

With the present paper, we wish to improve our understanding of single chain conformations in polymer networks at both preparation conditions and at swelling equilibrium. For this purpose, in Section 2 we analyze the samples of recent simulation studies<sup>[10,28]</sup> in more depth. Afterwards, in Section 3 we focus on the preparation state, and in Section 4 on the swelling equilibrium. In the latter section, we show that the chain size at swelling equilibrium emerges from the combination of an enlarged mobility of the network junctions and a nearly affine swelling of the non-fluctuating elastic part of the network strands. Throughout the analysis, these results are put into the context of existing literature. Finally, we present our conclusions in Section 5.

## 2. Simulation Data and Analysis

For analyzing the preparation state, we focus on the end-linked model networks simulated in ref. [10] with the Bond Fluctuation Model (BFM)<sup>[29,30]</sup> as these simulations rely on the same synthesis scheme as recent experimental data.<sup>[12]</sup> These networks cover a range of polymerization degrees  $N = 8, 16, 32, 64$  and different junction functionalities (maximum number of strands that are joined in a junction)  $f = 3, 4, 6$ . We analyze the size of the square internal distances between monomers  $j$  and  $k > j$  of all chains in real space. Such a computation relies on all  $N - s$  pairs along a chain with  $s = k - j$ , using

$$R^2(s) = \frac{1}{Z(N-s)} \sum_Z \sum_{j=1}^{N-s} (\mathbf{r}_j - \mathbf{r}_{j+s})^2 \quad (1)$$

where  $\mathbf{r}_j$  is the position vector of monomer  $j$ , and the first sum runs over all  $Z$  chains. Improved averaging is obtained by considering five independent replicas of each network. Moreover, we compute the square end-to-end distance,

$$R_e^2 = \frac{1}{Z} \sum_Z (\mathbf{r}_1 - \mathbf{r}_N)^2 \quad (2)$$

and the square radius of gyration,

$$R_g^2 = \frac{1}{ZN^2} \sum_Z \sum_{j=1}^N \sum_{k=j}^N (\mathbf{r}_j - \mathbf{r}_k)^2 \quad (3)$$

This analysis in real space is complemented by a computation of the scattering intensity of the individual chains

$$I(\mathbf{q}) = \frac{1}{ZN} \sum_{k=1}^Z \left| \sum_{j=1}^N e^{i\mathbf{q} \cdot \mathbf{r}_j} \right|^2 \quad (4)$$

as a function of the scattering vector  $\mathbf{q}$ . Here, we choose a scattering amplitude of unity for all  $N$  monomers along each chain, resulting in a normalization  $I(0) = 1$ . Moreover, we perform an isotropic averaging of the scattering vectors leading to  $\mathbf{q} \rightarrow |\mathbf{q}|$  and present all data as a function of  $q$ . Similar to the experiment,<sup>[12]</sup> we fit the scattered intensity  $I(q)$  to a Debye function for a Gaussian coil,

$$I_D(q) = I(0) \left( \frac{2}{Y^2} \right) (\exp(-Y) + Y - 1) \quad (5)$$

with  $Y = (qR_D)^2$ , where  $R_D$  refers to the radius of gyration as estimated from the Debye function. Additionally, we use the Guinier approximation

$$I_C(q) = I(0) \exp\left(-\frac{q^2 R_G^2}{3}\right) \quad (6)$$

to extract the corresponding Guinier estimate for the square radius of gyration,

$$R_G^2 \cong -3 \ln(I(q))/q^2 \quad (7)$$

from the data with  $qR_G \lesssim 1$ . A comparison of scattering data with an analysis in real space allows to check for the impact of deviations from perfectly ideal chain conformations and finite  $N$  effects.

In ref. [12], the authors had to estimate the portion of pending loops in order to extrapolate towards the estimated size of the chains connecting different junctions and not forming pending loops. In the simulations, we can determine the elastically active material (see refs. [31, 32] for a definition), and we restrict the analysis to all chains that are elastically active. This ensures that a) no pending loops are considered, b) we analyze only those chains that contribute to the modulus of the network, and c) all analyzed chains are connected to network junctions on both ends for collecting the full effect of the expected changes<sup>[10]</sup> in conformations. Thus, on top of removing pending loops from the analysis, we disregard also all other structures that play no role for network elasticity.

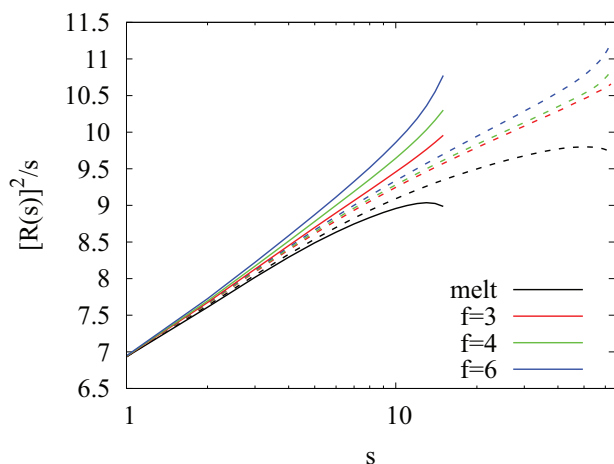


**Figure 1.** Normalized square size  $R^2(s)/s$  of chain sections containing  $s$  segments along the chain contour in the melt, and when end-linking the melt chains by  $f = 3, 4,$  and  $6$ -functional junctions. Two sets of data are shown for  $N = 16$  (continuous lines) and  $N = 64$  (dashed lines).

For analyzing the swelling process in Section 4, we build on the series of samples discussed in ref. [28]. These were prepared from two batches of hetero-complementary coupled star polymers providing network strands containing  $N = 23, 43,$  and  $82$  segments, respectively. For these samples, the coupling scheme suppresses the formation of pending loops.<sup>[33,34]</sup> Networks were prepared from equilibrated star polymer solutions over a large range of different polymer volume fractions at preparation,  $\phi_0$ . Boundary effects are corrected by replacing the nominal volume fraction  $\phi_0$  by an effective volume fraction,  $\phi_1$ . The set of all 38 available networks taken from our preceding paper is described in Table 1 of ref. [28]. The conversions of all samples are identical,  $p = 0.95$ , eliminating additional dependencies of  $p$  on the polymer volume fraction  $\phi$  in the samples. For a total number of  $M$  star polymers, this leads to a number of  $Z = pfM/2$  network chains formed by the bonds connecting pairs of stars. For all of these chains, we perform the analysis described above. Moreover, we use the data on the cross-link motion and on the time average strand size published in our preceding work<sup>[28]</sup> for a more detailed analysis of the swelling process.

### 3. Preparation Conditions

As discussed in the introduction, both the polymer architecture and the assembly process play a role in the enlargement of the strand size in the networks. Hence, we compare the data of ref. [12] on end-linked model networks with the simulations in our recent study<sup>[10]</sup> on the same class of networks. Chain conformations in monodisperse polymer melts were taken from a preceding study.<sup>[9]</sup> In Figure 1, we analyze the square size of chain sections,  $R^2(s)$ , containing  $s$  segments inside a single network strand of the elastically active material of the networks or inside a chain in the corresponding melt. As shown in Figure 1, the network chains are extended with respect to  $R^2(s) \propto s$  and with respect to the corresponding melt. The extension grows as a function of  $s$ , whereby the difference is most pronounced next to

the chain ends bound to a junction. Here, the additional contacts to the connected network strands across the network junction have a major impact.<sup>[10]</sup> For small  $s$ , this effect is averaged out by considering all chain sections containing  $s$  segments, see Equation (1). For  $s = 1$ , the data show the mean square size of a bond in the simulation model, which is close to seven for the BFM at melt conditions.<sup>[8]</sup>

When analyzing chains by scattering techniques, the internal distances are averaged according to their frequency of occurrence. Therefore, the less frequent sections over the full contour length enter with a lower weight into the average. Thus, only a part of the total enlargement of the full end-to-end vector of the network strands is accessible from the scattering data. Moreover, Figure 1 shows that the chain conformations are significantly non-ideal as  $R^2(s)/s$  is not constant. Therefore, it is also instructive to see how accurately the true strand size can be captured by the scattering data of the labeled chains when analyzing these by standard methods like the Debye or the Guinier approximation. This latter test is performed in the Appendix, showing that the Debye approximation leads to a more accurate estimate of the chain size.

In order to evaluate the impact of the cross-linking reaction on the chain conformations in a similar manner as in the experiment, we compute the single chain scattering function of strands in networks and in the corresponding melts. We use the Debye function, Equation (5), to estimate the squared radius of gyration from the scattering data. In order to reduce the impact of non-ideal chain conformations on this estimate, we consider only data with  $qR_D < 1$  corresponding to  $I(q) > 0.736$ , see the Appendix for more details. Finally, from the Debye estimates for the radii of gyration of chains in networks and melt, we compute the enlargement factor

$$\alpha = \frac{R_{D,net}^2}{R_{D,melt}^2} \quad (8)$$

as in ref. [12], which is the ratio of the squared radius of gyration of the network strands,  $R_{D,net}^2$ , and the squared radius of gyration of melt chains,  $R_{D,melt}^2$ . Regarding network elasticity, we actually require  $\alpha$  as determined from  $R_e$ . As shown in the Appendix, there are different coefficients connecting  $R_D$  and  $R_e$  when comparing chains in melts and chains in networks. Thus, in order to estimate the impact on the elastic behavior, we alternatively compute  $\alpha$  based upon the corresponding ratios of the  $R_e$  data.

For placing the data for  $\alpha$  onto the same concentration scale as in ref. [12], we estimate  $R_e^2 \approx 6R_{D,melt}^2$ , and we use the concentration of chains per volume,  $c = \phi/(v_0N)$ , where  $\phi = 0.5$  is the average occupation of monomers on the lattice,  $v_0 = 8u^3$  the volume of a monomer in unit volumes of the lattice, and  $N$  the degree of polymerization of the chains. For consistency reasons, when calculating  $cR_e^3$ , we rely either on  $R_D$  as measured from the scattering data, or on  $R_e$  as computed in real space. The apparent shift between both sets of data along the horizontal axis in Figure 2 results from systematic corrections of the estimate  $R_e^2 \approx 6R_{D,melt}^2$  arising from different bond–bond correlation corrections<sup>[8]</sup> and from mathematical corrections (of order  $1/N$ ) when computing  $R_g$  and  $R_e$  from a finite set of discrete coordinates, see also Figure A3 and the discussion in the Appendix.

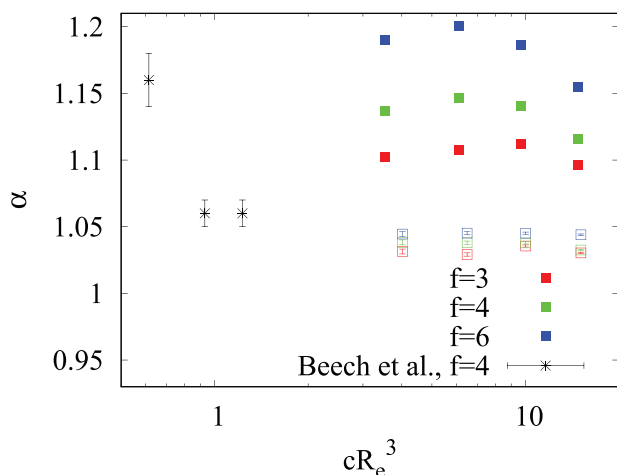


**Figure 2.** Enlargement factors according to Equation (8) as computed from radii of gyration  $R_D$  derived from scattering data (hollow symbols) and from an analogue ratio relying on end-to-end vectors (full symbols), together with SANS data taken from Table 1 of Beech et al.<sup>[12]</sup> (asterisks: Debye prestrain data). Error bars of our scattering data refer to the numerical error of the data fit. The statistical error of the data of the present study (due to the limited number of chain conformations) is below 2% and not indicated in the Figure.

In Figure 2, our scattering analogue estimate of  $\alpha$  based upon  $R_D$  produces data continuing the trend found by Beech et al.<sup>[12]</sup> toward larger  $cR_e^3$ . The comparison between the  $R_D$  based scattering data and a direct evaluation of  $R_e$  indicates that most of the chain enlargement is missed in scattering experiments. Thus, we expect that the data of ref. [12] provide only a lower bound for the true enlargement factor of the end-to-end distances of the chains. The latter, however, control the limit of very large deformations and the elasticity of the network. For the limit of  $cR_e^3 \rightarrow \infty$ , a convergence of  $\alpha \rightarrow 1$  can be expected,<sup>[10]</sup> as indicated by the trend of the data with the largest  $cR_e^3$ . For networks prepared from melts as in our simulation study, the limit  $cR_e^3 \rightarrow 1$  is equivalent to  $N \rightarrow 1$  where the chains loose their ability to stretch (see also the limit  $s \rightarrow 1$  in Figure 1). For networks prepared from long chains at low concentrations around  $cR_e^3 \approx 1$ , this restriction does not hold, as evident from the experimental data of ref. [12].

It is important to emphasize that the total chain enlargement,  $\alpha$ , consists of a swelling and a stretching contribution as discussed in ref. [10]. The swelling contribution arises from additional bond–bond correlations across the network junctions. These affect mainly the conformations near the chain ends and lead in first approximation to a renormalization of the chain size. The stretching contribution causes a further enlargement of the chain size with respect to this reference size. Only the stretching contribution leads to an enlargement of the shear modulus. Therefore, our  $R_e$  data serve as an upper bound of the true impact on the elasticity of the networks, and more accurate predictions for the reference chain size are required. In this respect, Figure S2 (Supporting Information) of ref. [10] is useful, as it allows for a rough estimate of the contributions of swelling and stretching to  $R_e^2$ . According to this Figure, swelling becomes more relevant for smaller  $N$  and larger  $f$ , suppressing in part the stretching contribution of the enlarged chain size.

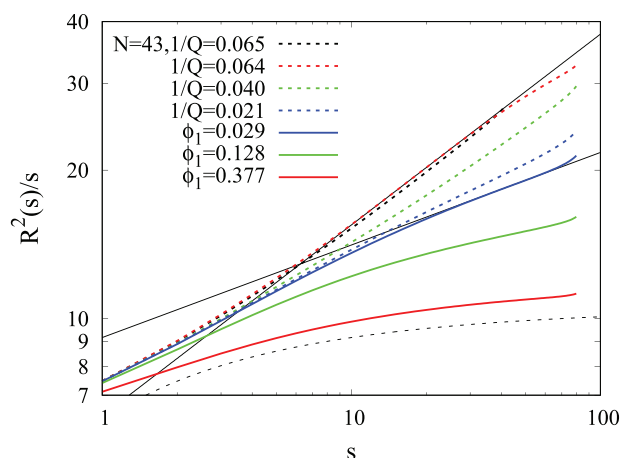


**Figure 3.** Square size  $R^2(s)$  of internal chain sections containing  $s$  segments for the  $N = 82$  samples of Figure 4 and one additional data set for  $N = 43$  at  $1/Q = 0.065$  (black dashed line). The black dashed line at the bottom refers to the melt limit at  $\phi = 0.5$  (Equation (10) of ref. [8]). The continuous black lines show power law fits to the increase of  $R^2(s)$  at preparation conditions ( $\phi_1 = 0.029$ ,  $\nu = 0.594 \pm 0.001$  around  $s = 45$ ) and to the steepest increase at swelling equilibrium ( $1/Q = 0.064$ ,  $\nu = 0.694 \pm 0.001$  around  $s = 17$ ).

## 4. Swelling Equilibrium

As summarized in the introduction, to date the swelling process of individual network strands is still not fully understood. Several competing concepts have been proposed, leading to similar predictions. Moreover, the limited accuracy of the available scattering data in literature does not allow for a clear distinction between the model predictions. In order to shed more light into this problem, we computed  $R^2(s)$  for all star networks of our recent study, and in Figure 3, we present data for the largest chain length between connected star centers,  $N = 82$ , at three effective polymer volume fractions at preparation,  $\phi_1$ , see ref. [28] for more details. The data in Figure 3 refer to the largest polymer volume fraction of this series of samples ( $\phi_1 = 0.377$ ), a sample close to the overlap volume fraction of the star polymers ( $\phi_1 = 0.029$ ), and one data set at an intermediate  $\phi_1$ , indicating the transition between these limits. The data at the highest  $\phi_1$  largely follow the reference for the melt limit at  $\phi = 0.5$ .<sup>[8]</sup> A substantial deviation occurs around  $s = 1$ , since the root mean square bond length  $b = R(1)$  changes significantly for large  $\phi$ , whereas in Figure 3, it becomes merely constant for the lower  $\phi_1$  at preparation and  $\phi = 1/Q$  in swelling equilibrium, see also Figure 3 of ref. [35]. Changes toward  $s \rightarrow N$  are related to modified chain conformations, undergoing a transition from the concentrated regime towards the semi-dilute limit in the preparation state. At the largest polymer volume fraction ( $\phi_1 = 0.377$ ), the large  $s$  behavior approaches a constant, indicating random walk statistics for large  $s$ . In contrast, the data close to overlap volume fraction ( $\phi_1 = 0.029$ ) fits better to a power law growth  $R(s) \propto s^\nu$ , with  $\nu = 0.594 \pm 0.001$  for  $s \geq 10$ , not far from the expected value  $\nu \approx 0.587597(7)$ .<sup>[36]</sup>

Samples at a polymer volume fraction of  $\phi = 1/Q$  refer to networks at swelling equilibrium, as indicated by the equilibrium degree of swelling,  $Q$ . For these samples, we see a cross-over from the good solvent limit with  $\nu \approx 0.62$  at low polymer volume

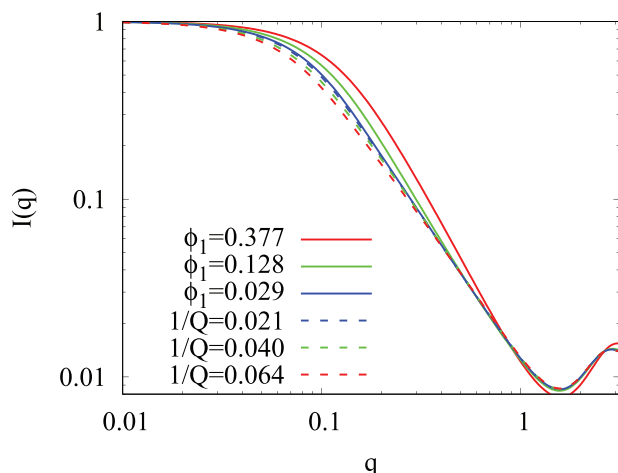


**Figure 4.** Single chain form factors in star networks with  $N = 82$  and different effective  $\phi_1$  at preparation conditions (continuous lines) or  $\phi = 1/Q$  at swelling equilibrium (dashed lines). The same color is used for data of the same networks at preparation and swelling equilibrium, see ref. [28] for more details on the samples.

fraction ( $1/Q = 0.021$ ) toward an exponent  $\nu = 0.694 \pm 0.001$  at the highest polymer volume fraction ( $1/Q = 0.064$ ) for the  $N = 82$  data with the steepest increase in  $R(s)$ . This latter exponent reproduces the result  $\nu \approx 0.7$  of the arrested swelling of single chain globules.<sup>[19,20]</sup> We do not observe an explicit scaling  $R \propto N$  as proposed in ref. [21]. It appears that the effective scaling is solely a function of  $\phi$  at swelling equilibrium, since networks made of shorter chains locking in at the same  $Q$  develop similar chain conformations at intermediate  $s$ , see Figure 3 for an example (the uppermost two sets of data). The transition point from swollen conformations at small  $s$  to more extended conformations at intermediate  $s$  shifts toward larger  $s$  for decreasing  $\phi = 1/Q$  at swelling equilibrium, in qualitative agreement with the expected growth of the blob size (compare e.g., data at  $1/Q = 0.04$  and  $1/Q = 0.064$ ). In ref. [22], it was hypothesized that the appearance of such a transition indicates the possibility of a local strand separation upon swelling, which would lead to the appearance of the two scaling regimes proposed by Panyukov and Rubinstein.<sup>[18]</sup> Our data are in agreement with this picture, once a sufficiently large volume change from the preparation state occurs.

In Figure 4, we present the single chain form factors for the samples of Figure 3 with the largest  $N$ . These form factors qualitatively reproduce the behavior observed in real space: near the overlap threshold, there is almost no change between equilibrium swelling and preparation conditions, whereas preparation at larger overlap of the polymers leads to an increased deformation of the chains upon swelling. For a rough quantitative orientation, one can consider that a chain section of  $s$  monomers produces roughly a scattering intensity of  $s/N$  for the normalized data in Figure 4. We use this estimate to analyze sections of the scattering function complying with a specific range of  $s$  analyzed in real space. One should also note that scattering data at a certain  $q$  arise from real space data over a significant range of  $s$ , with an average size on the corresponding length scale. Vice versa, length information for a particular  $s$  is smeared out over a broad

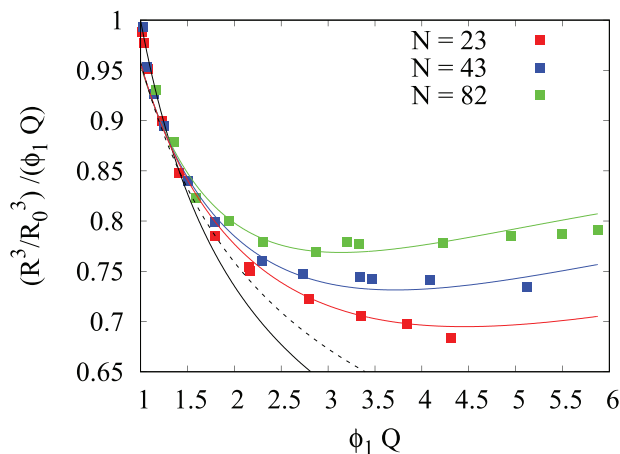


**Figure 5.** Swelling of individual chains,  $(R/R_0)^3$ , normalized by the volume change upon swelling from the preparation state,  $\phi_1 Q$ . Data taken from ref. [28]. The black continuous line is the phantom model prediction, Equation (10), for  $f = 4$ . The black dashed line is the model prediction for all  $N$  considering only enlarged cross-link fluctuations due to swelling but no entanglement contributions. The colored lines are the model predictions for entangled chains, Equation (16), using the parameters of preceding work.<sup>[28]</sup>

range of wavevectors. Moreover, the cross-over from  $I(q) \approx 1$  at small  $q$  toward  $I(q) \propto q^{1/\nu}$  impacts significantly the data for  $I(q) \geq 0.2$ . Therefore, we restrict the analysis of the asymptotic exponent  $1/\nu$  of the data in Figure 4 to the intensity range  $0.02 < I(q) < 0.2$ .

From the scattering data for the sample with  $1/Q = 0.064$ , we obtain an exponent of  $\nu \approx 0.655 \pm 0.002$  from a power law fit,  $I(q) \propto q^{1/\nu}$ , about 6% below the steepest slope of  $\nu = 0.694 \pm 0.001$  derived from the real space extension  $R(s)$ , indicating that the scattering intensity arises from a broader range of chain stretches  $s$  with a somewhat smaller exponent governing the dependence of  $R(s)$ . For a polymer volume fraction at preparation of  $\phi_1 = 0.029$  close to overlap conditions, our analysis of the scattering data produces  $\nu \approx 0.602 \pm 0.001$ , that turns into an apparent  $\nu \approx 0.608 \pm 0.001$  at swelling equilibrium, again somewhat below the steepest increase of the real space data. Altogether, the true steepest increase of  $R(s)$  at swelling equilibrium is systematically underestimated by an analysis of the scattering data due to the different sampling of the data in real and reciprocal space. Finally, we have to mention that an Ornstein Zernike function generalized to a fractal dimension  $1/\nu$ <sup>[37]</sup> fitted to the same range of  $I(q)$  does not produce a more accurate estimate of  $\nu$  than the simple power law fit employed above.

As compared to the change of volume upon swelling,  $\phi_0 Q$ , the swelling of individual chains is less than predicted by the affine model,  $(R^3/R_0^3)/(\phi_0 Q) = 1$ , once significant swelling sets in, see Figure 5. Note that we used the effective polymer volume fraction at preparation conditions  $\phi_1$  (replacing  $\phi_0$ , see ref. [28] for details) for the Figure in order to remove boundary effects. A sub-affine deformation of network strands was observed first in ref. [38] and corroborated by a study on labeled paths in randomly cross-linked networks.<sup>[39]</sup> In both cases, only a part of the samples showed agreement with estimates<sup>[40]</sup> based upon the phantom model similar to Figure 5. In general, only the time average extension of the network strands deforms affinely,<sup>[41–43]</sup>

which holds in a reasonable approximation for our model networks, see Figure 1 of ref. [28]. This point was missed in several studies,<sup>[44–46]</sup> causing some confusion about the degree of affinity of the swelling process. NMR data referring to time average extensions also supports an affine swelling process for larger degrees of swelling.<sup>[47,48]</sup> Similar to these findings, a constant level of  $(R^3/R_0^3)/(\phi_0 Q)$  in Figure 5 indicates an enforced affine swelling process beyond a threshold swelling, hinting simultaneously toward a possible incomplete conformational averaging of the NMR data as observed in ref. [49] for low solvent content. The fluctuating part of the strand size is related to the motion of the cross-links, and thus, it is restricted by all constraints acting on them.<sup>[50]</sup> Upon swelling, these constraints are partially released,<sup>[28,51]</sup> leading to a complex sub-affine change of the extension of the network strands.

For the limit of small  $\phi_0 Q$ , we expect a negligible effect of entanglements. Let us assume an ideal network of monodisperse Gaussian strands connected by  $f = 4$  functional junctions for which we employ the phantom model<sup>[52,53]</sup> for a first rough estimate. In the phantom model, the square chain size,  $R^2$ , is split into a fluctuating and a time average contribution:<sup>[7,51,53]</sup>

$$R^2 = 2\delta R^2 + \langle R \rangle^2 \quad (9)$$

Since each network chain has a network junction at each end, the fluctuating contribution is twice the mean square displacement  $\delta R^2$  of a network junction analyzed in preceding work. Let us introduce an index “0” to denote the preparation state. For the ideal network of Gaussian chains, the fluctuating part is  $2\delta R^2/R^2 = 2\delta R_0^2/R_0^2 \approx 2/f$  and remains independent of the degree of swelling. For Gaussian chains, the root mean square size of a Kuhn segment does not change during swelling,  $b_0 = b$ . The time average part of the square chain size is  $\langle R_0 \rangle^2/R_0^2 = (f - 2)/f$  at preparation conditions. Upon swelling, this time average contribution expands affinely, i.e., by a factor of  $(\phi_0 Q)^{2/3}$ . Thus, we expect

$$\begin{aligned} \frac{1}{\phi_0 Q} \frac{R^3}{R_0^3} &= \frac{1}{\phi_0 Q} \left( \frac{2\delta R^2 + \langle R \rangle^2}{2\delta R_0^2 + \langle R_0 \rangle^2} \right)^{3/2} \\ &= \frac{1}{\phi_0 Q} \left( \frac{2 + (f - 2)(\phi_0 Q)^{2/3}}{f} \right)^{3/2} \end{aligned} \quad (10)$$

at small  $\phi_0 Q \approx 1$ . In Figure 5, the respective line for  $f = 4$  demonstrates that this estimate agrees well with the simulation data at small  $\phi_0 Q$ . Recall that the co-complementary coupling of our star model networks leads to comparatively small changes in the connectivity of the samples within the overlap regime,  $\phi > \phi^*$ , see Figure 2 of ref. [28]. Other network architectures are more susceptible to defects as a function of  $\phi_0$ , enlarging the fluctuating part of the chain size. At small  $\phi_0 Q \gtrsim 1$  this may cause a faster decay than predicted.

For  $\phi_0 Q \gtrsim 2$ , the data in Figure 5 increasingly deviate from the prediction according to Equation (10) toward a more affine behavior for increasing  $N$ . Here, entanglements significantly impact the behavior, and we generalize the above estimate regarding entangled systems. For simplicity, we discuss only the a-thermal limit of the simulation data. Generalization toward theta or good

solvents is straightforward, requiring only that all expressions related to size or fluctuating size are replaced by the corresponding textbook expressions. We drop corrections arising from a possible dependence of the Kuhn segment size on polymer volume fraction. Furthermore, we use the confinement degree of polymerization,  $N_c$ , to describe the width of the confining tube, see ref. [54] for more details. In Equation (10) of ref. [28], we derived an expression for  $\delta R_0^2$  that was tested with simulation data for  $N = 82$ . Inserting the scaling predictions for the exponents of  $\phi_0$ , this equation can be rearranged into

$$\delta R_0^2 \approx \frac{b_0^2 N \phi_0^{-(2\nu-1)/(3\nu-1)}}{\frac{f(f-2)}{f-1} + \frac{fN}{2N_c} \phi_0^{(2-2\nu)/(3\nu-1)}} \quad (11)$$

here, the first term in the denominator models the confinement due to the network connectivity acting on the cross-links, the second part of the denominator containing  $N_c$  describes the entanglement contribution to these constraints, while the enumerator is the chain size in the corresponding solution as reference state. Entanglement constraints are removed by setting  $N_c = \infty$ , allowing for a separation of both contributions. Furthermore, in Figure 4 of ref. [28], we showed that cross-link mean displacements change upon swelling according to

$$\frac{\delta R^2}{\delta R_0^2} \propto (\phi_0 Q)^\beta \quad (12)$$

with  $\beta = 0.25 \pm 0.01$ .<sup>[28,55]</sup> The time average contribution to chain size is estimated from Equation (9) through a fit to the a-thermal limit of the scaling model<sup>[6,56]</sup> for the instantaneous size of a polymer in a semi-dilute solution,  $R_0$ . This provides

$$\begin{aligned} \langle R_0 \rangle^2 &= R_0^2 - 2\delta R_0^2 \\ &\approx z b_0^2 N \phi_0^{-(2\nu-1)/(3\nu-1)} - 2\delta R_0^2 \end{aligned} \quad (13)$$

for an excluded volume of  $\nu \approx b^3$  as in our simulations. In practice, one can determine  $R_0^2$  from single chain scattering in the preparation state. The data of ref. [28] for the three different  $N$  fit to a coefficient of  $z = 1.62 \pm 0.02$ . The time-average part of chain size deforms in an almost perfectly affine fashion upon swelling,

$$\frac{\langle R \rangle^2}{\langle R_0 \rangle^2} \approx X (\phi_0 Q)^{2/3} \quad (14)$$

as can be seen from the coefficient  $X \approx 0.94$  that we determined as a best fit to the  $N = 82$  data of Figure 1 of ref. [28] at high overlap of the star polymers. Let us use the ratio

$$\begin{aligned} Z(\phi_0) &= \frac{\langle R_0 \rangle^2}{2\delta R_0^2} \\ &= \frac{zf}{2} \left( \frac{f-2}{f-1} + \frac{N}{2N_c} \phi_0^{(2-2\nu)/(3\nu-1)} \right) - 1 \end{aligned} \quad (15)$$

for a compact notation of the model prediction for entangled networks:

$$\frac{1}{\phi_0 Q} \frac{R^3}{R_0^3} = \frac{1}{\phi_0 Q} \left( \frac{(\phi_0 Q)^\beta + X (\phi_0 Q)^{2/3} Z(\phi_0)}{1 + Z(\phi_0)} \right)^{3/2} \quad (16)$$

This expression is tested with the simulation data by using  $N_c \approx 19.4$  and the effective  $f \approx 3.68$  provided in ref. [28]. Note that these parameters were fit to the  $N = 82$  data only, but allowed a reasonable description of all data at large  $\phi_0$ . We apply the same strategy and fit the effective  $\phi_1$  in Table 1 of ref. [28] for  $N = 82$  as a function of  $\phi_1 Q$  to express the theoretical  $\phi_0$  in Equation (15) as a function of  $\phi_1 Q$  for the plot. The agreement between the data in Figure 5 and Equation (16) demonstrates the consistency of our analysis as no additional fit parameter is needed to approximate the data. The trend of the simulation data as a function of  $N$  is supported by our derivation above:  $Z(\phi_0)$  becomes more concentration dependent and larger for increasing  $N$ , pushing the data closer to the affine limit of  $(R^3/R_0^3)/(\phi_0 Q) = 1$ , which is the expected asymptotic limit for  $N \rightarrow \infty$ . In Figure 5, the dashed line according to Equations (15) and (16) in the limit of  $N_c \rightarrow \infty$  reveals the contribution of the enlarged cross-link fluctuations upon swelling when comparing with the phantom limit. This contribution is independent of  $N$  for constant  $f$ , similar to the phantom model prediction, since all dependencies on  $N$  cancel out once the entanglement contribution is removed. The remaining difference to the simulation data shows the effect of the entanglements. Finally, we have to remark that  $f \approx 3.68$  refers to an average over the range of volume fractions fit for the  $N = 82$  data in ref. [28]. A more detailed analysis shows that  $f$  decays weakly as a function of  $\phi$  for the volume fractions of interest. The corresponding correction for large  $\phi_1 Q$  is comparable to the size of the data symbols for our network architecture due to the suppression of pending loops. However, for conventional end-linked model networks, a more detailed analysis of this point could become necessary.

Equation (16) and the above discussion show that a combination of NMR and scattering techniques could be used to gain a deeper insight into the swelling behavior of the network strands. Time average extensions in the non-affine limit<sup>[28]</sup> are available in proton multiple quantum NMR techniques,<sup>[57]</sup> while instantaneous sizes can be measured by scattering, providing access to the constraints acting on the network junctions,  $\delta R^2$ . However, obtaining sufficiently accurate data is highly challenging. In Figure 6, we plot the only available data set in literature where the size of individual strands was determined in both the preparation state and at swelling equilibrium.<sup>[14,38]</sup> The error is quite large, so that conclusions from the data are difficult. Moreover, the experimental data seem to drop below the phantom model prediction. The latter is an indication that the true degree of branching,  $f$ , could be significantly below the expected  $f$  that was used for plotting the theoretical lines. Such a reduction could result from a large portion of pending loops, which are suppressed in our hetero-complementary coupled model networks<sup>[33,34]</sup> but not in the end-linked model networks of refs. [14, 38].

Altogether, the above analysis contributes to our understanding of the chain conformations and the constraints acting on the network junctions during swelling. Our results demonstrate that the chain size in networks swollen to equilibrium emerges from the preparation conditions along two mechanisms: first, the enlarged mobility of the network junctions allowing for larger fluctuations in chain size, and second, a nearly affine deformation of the time-average component of the chain extension. A description of the time-average and the fluctuating component of the conformations of the network strands is the basis to understand

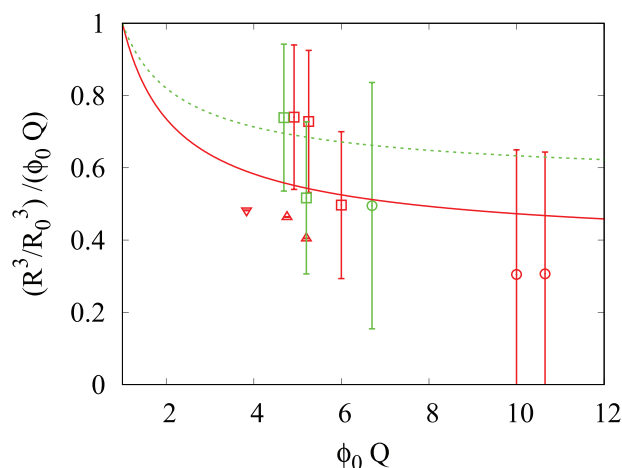


**Figure 6.** Experimental data of refs. [14, 38] for the subaffine swelling of network strands. Data points refer to  $f = 6$  (green) and  $f = 4$  (red), and lines correspond to Equation (10) for  $f = 6$  (green) and  $f = 4$  (red). The molar mass of the deuterated chains was  $M_n \approx 23$  kDa (squares),  $M_n \approx 10.5$  kDa (spheres),  $M_n \approx 6.5$  kDa (triangles),  $M_n \approx 3.1$  kDa (triangles upside down), respectively. The error of the measurement was provided only for some samples in the second work.<sup>[38]</sup> A similar accuracy was assumed for the first measurement<sup>[14]</sup> to estimate the total error of these data.

the deformation behavior of networks and gels at swelling equilibrium. Even though our networks were designed for the non-entangled limit, a significant impact of entanglements is already visible, see Figure 5. Thus, a modeling of swollen networks and gels including both contributions from entanglements and the cross-linked network structure (phantom contribution) appears to be necessary for understanding the properties at the swelling equilibrium. A more detailed test of the theory in the entangled regime has to be postponed until data for a broader range of  $N$  becomes available.

## 5. Conclusion

In this work, we have used large scale computer simulations to explore the conformations of network strands in end-linked model networks and to analyze the swelling of the network strands in model networks built from star polymers. Our data on the end-linked model networks corroborate the finding of ref. [12], claiming that the chain conformations inside a network do not entirely agree with the reference conformations of the corresponding polymer melt prior to cross-linking. Instead, there are measurable changes in the equilibrium size of the network strands. These contain stretching and swelling contributions, where the former control the change in modulus, whereas the latter dominate the renormalization of the equilibrium strand size due to the cross-linking process. Hence, the measured enlargement of the chain size results in an overestimate of the corresponding increase in modulus. This increase is best analyzed in computer simulations because experimental chain sizes derived from scattering data reveal only a part of the true chain enlargement. More precise predictions for estimating the true reference chain at preparation conditions size are still lacking, which hampers a more detailed analysis of the impact on network modulus at preparation conditions.

The swelling of chain size is weakly sub-affine, and it is larger than predicted by the phantom model. This behavior arises from a partial suppression of the cross-link fluctuations by entanglements in the preparation state and from the subsequent growth of these fluctuations with the swelling of the samples, in contrast to the fluctuations of Gaussian chains remaining independent of the state of strain.

The elastic contribution to the chain size swells nearly affinely. In combination, this leads to a chain size in the swollen network that lies in between the phantom model prediction and the affine limit. Predictions for the swollen chain size can be made after considering the change in the cross-link motion upon swelling. These latter predictions are relevant for testing and developing more precise models describing the deformation behavior of swollen networks.

## Appendix A

**Figure A1** shows the swelling of the internal distances along the chain contour,  $R_s^2(s)$  and the enlargement factors of square chain size,  $\alpha$ , when analyzed from a topology blind average over all chains. We observe a signifi-

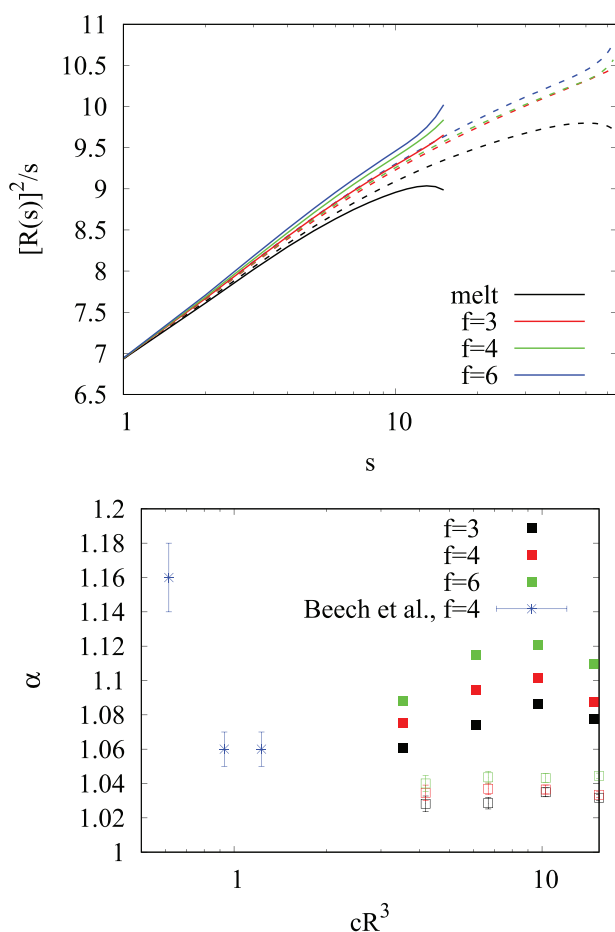


**Figure A1.** “Topology blind” analysis of chain conformations considering all chains in the system (no distinction between pending chains, pending loops, or active chains in contrast to the main text). Upper part: same analysis as in Figure 1 for all chains; lower part: same analysis as in Figure 2 for all chains.

**Table A1.** Data for the average size of the network strands.  $R_D$ : fit of the scattering data  $I(q)$  with the Debye function, Equation (5), over interval  $qR_D < 1$  corresponding to  $I(q) > 0.736$ ;  $R_G$ : fit of the scattering data with the Guinier approximation according to Equation (7) over interval  $qR_G < 1$  corresponding to  $I(q) > 0.717$ .  $R_g$  and  $R_e$  are directly computed from the coordinates of the chain monomers.

| sample     | $R_D$ [ $\mu$ ] | $R_G$ [ $\mu$ ] | $R_g$ [ $\mu$ ] | $R_e$ [ $\mu$ ] |
|------------|-----------------|-----------------|-----------------|-----------------|
| melt, N=8  | 3.272(2)        | 3.184(3)        | 3.247           | 7.679           |
| f=3, N=8   | 3.323(1)        | 3.230(2)        | 3.552           | 8.062           |
| f=4, N=8   | 3.334(1)        | 3.240(2)        | 3.579           | 8.187           |
| f=6, N=8   | 3.344(1)        | 3.249(2)        | 3.619           | 8.378           |
| melt, N=16 | 4.836(2)        | 4.696(5)        | 4.799           | 11.61           |
| f=3, N=16  | 4.906(1)        | 4.765(3)        | 5.069           | 12.22           |
| f=4, N=16  | 4.927(1)        | 4.785(3)        | 5.111           | 12.43           |
| f=6, N=16  | 4.944(1)        | 4.806(3)        | 5.159           | 12.72           |
| melt, N=32 | 7.041(2)        | 6.845(7)        | 6.994           | 17.06           |
| f=3, N=32  | 7.165(1)        | 6.960(5)        | 7.284           | 17.99           |
| f=4, N=32  | 7.173(1)        | 6.967(5)        | 7.314           | 18.22           |
| f=6, N=32  | 7.198(1)        | 6.989(5)        | 7.375           | 18.58           |
| melt, N=64 | 10.168(2)       | 9.88(2)         | 10.111          | 24.75           |
| f=3, N=64  | 10.321(1)       | 10.023(7)       | 10.418          | 25.91           |
| f=4, N=64  | 10.332(1)       | 10.032(7)       | 10.447          | 26.14           |
| f=6, N=64  | 10.389(1)       | 10.085(7)       | 10.531          | 26.60           |

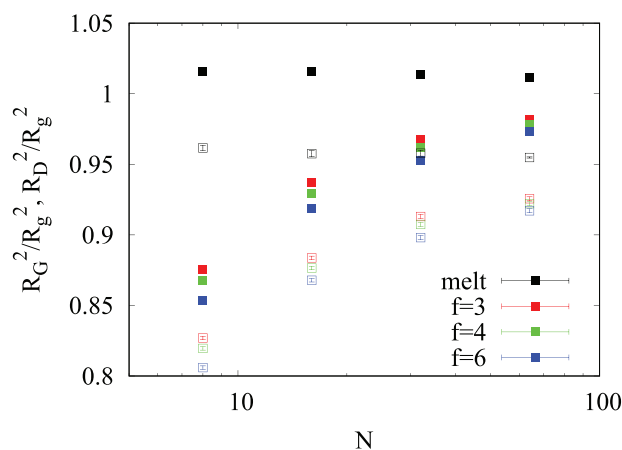


**Figure A2.** Comparison of different estimates for the radius of gyration from scattering data,  $R_G$  (hollow symbols) and  $R_D$  (filled symbols) with the direct computation of  $R_g$ .

cant reduction of chain swelling as compared to the analysis focusing on the elastically active material alone, see Figures 1 and 2.

In **Table A1**, we present the estimates of the radius of gyration as obtained by analyzing the scattering functions computed from the coordinates of the network strands. Here, either the Debye function, Equation (5), was used for a fit over the interval  $qR_D < 1$  corresponding to  $I(q) > 0.736$ , or the Guinier approximation according to Equation (7) over the interval  $qR_G < 1$  corresponding to  $I(q) > 0.717$ . Moreover, **Table A1** also contains the results from a direct computation of the radius of gyration,  $R_g$ , or the end-to-end vector,  $R_e$ , from the coordinates of the chain monomers. The Guinier fit seems to have a precision better than 0.1%, but the wrong asymptotics of Equation (6) produces systematic deviations  $R_G < R_D$  from the Debye fit, similar to the trends of the data reported in previous work.<sup>[12]</sup> The comparison of both estimates with the “true”  $R_g$  in **Figure A2** shows that  $R_D$  is closer to the true  $R_g$  for all samples of our

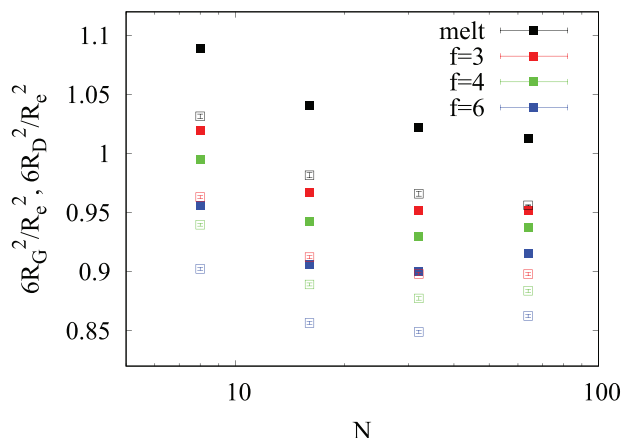


**Figure A3.** Comparison of different estimates for the radius of gyration from scattering data,  $R_G$  (hollow symbols) and  $R_D$  (filled symbols) with the end-to-end distances measurement in real space,  $R_e$ .

study. Moreover, both estimates based upon the scattering data lead to a systematically increasing underestimate for decreasing  $N$  and increasing  $f$ . The former is related to  $1/N$  corrections when comparing these different approaches (scattering vs direct computation) for determining the radius of gyration. The latter is related to the different statistical weights for large chain sections in both methods. The  $1/N$  corrections are mainly compensated when estimating  $R_e$  based upon the scattering data, see **Figure A3**, while most of the  $f$ -dependent correction survives. In general, we observe that the Debye function provides the more accurate estimate for  $R_e$  for all network data, while only the melt data at small  $N$  could be analyzed more accurately by using the Guinier approximation. Altogether, we conclude that  $R_D$  is the more appropriate measure of chain size. This is reflected in the main text by focusing on the  $R_D$  data.

## Acknowledgements

This work has received funding from the Deutsche Forschungsgemeinschaft (DFG) via project FOR2811 under grant 397384169. Computational resources provided by the Centre for Information Services and High Performance Computing (ZIH) of TU Dresden are gratefully acknowledged.

Open access funding enabled and organized by Projekt DEAL.

## Conflict of Interest

The authors declare no conflict of interest.

## Data Availability Statement

The data that support the findings of this study are available from the corresponding author upon reasonable request.

## Keywords

conformations, polymer gels, polymer networks, scattering, swelling

Received: January 12, 2024

Published online:

[1] C. Alvarez-Lorenzo, S. Anguiano-Igea, A. Varela-Garcia, M. Vivero-Lopez, A. Chncheiro, *Acta Biomater.* **2019**, *84*, 49.

- [2] F. B. A. Descallar, X. Yang, L. C. Geonzon, S. Matsukawa, *Food Sci. Technol. Res.* **2023**, *29*, 171.
- [3] G. Heinrich, M. Klüppel, *Adv. Polym. Sci.* **2022**, 289, 1.
- [4] A. P. More, *Polym. Bull.* **2024**, *81*, 1893.
- [5] M. Lang, *Nat. Mater.* **2023**, *22*, 1283.
- [6] M. Rubinstein, R. Colby, *Polymer Physics*, Oxford University Press, New York, **2003**.
- [7] M. Lang, *ACS Macro Lett.* **2018**, *7*, 536.
- [8] J. P. Wittmer, P. Beckrich, H. Meyer, A. Cavallo, A. Johner, J. Baschnagel, *Phys. Rev. E* **2007**, *76*, 011803.
- [9] M. Lang, M. Rubinstein, J.-U. Sommer, *ACS Macro Lett.* **2015**, *4*, 177.
- [10] M. Lang, T. Müller, *Macromolecules* **2022**, *55*, 8950.
- [11] M. Lang, *Macromol. Symp.* **2019**, *385*, 1800168.
- [12] H. K. Beech, J. A. Johnson, B. D. Olsen, *ACS Macro Lett.* **2023**, *12*, 325.
- [13] H. Benoit, D. Decker, R. Duplessix, C. Picot, P. Rempp, J. P. Cotton, B. Farnoux, G. Jannink, R. Ober, *J. Pol. Sci. B* **1976**, *14*, 2119.
- [14] M. Beltzung, C. Picot, P. Rempp, J. Herz, *Macromolecules* **1982**, *15*, 1594.
- [15] E. R. Duering, K. Kremer, G. Grest, *J. Chem. Phys.* **1994**, *101*, 8169.
- [16] N. R. Kenkare, S. W. Smith, C. K. Hall, S. A. Khan, *Macromolecules* **1998**, *31*, 5861.
- [17] P. Flory, J. Rehner Jr, *J. Chem. Phys.* **1943**, *11*, 521.
- [18] S. Panyukov, M. Rubinstein, *Macromolecules* **2005**, *38*, 3511.
- [19] M. Pütz, K. Kremer, R. Everaers, *Phys. Rev. Lett.* **2000**, *84*, 298.
- [20] N.-K. Lee, C. F. Abrams, A. Johner, S. Obukhov, *Macromolecules* **2004**, *37*, 651.
- [21] S. K. Sukumaran, G. Beaucage, J. E. Mark, B. Viers, *Eur. Phys. J. E* **2005**, *18*, 29.
- [22] N.-K. Lee, C. F. Abrams, A. Johner, S. Obukhov, *Phys. Rev. Lett.* **2003**, *90*, 225504.
- [23] S. K. Sukumaran, G. Beaucage, *Europhys. Lett.* **2005**, *59*, 714.
- [24] E. Mendes, P. Lindner, M. Buzier, F. Boué, J. Bastide, *Phys. Rev. Lett.* **1991**, *66*, 1595.
- [25] J. A. Hinkley, C. C. Han, B. Mozer, H. Yu, *Macromolecules* **1978**, *11*, 836.
- [26] M. Beltzung, C. Picot, J. Herz, *Macromolecules* **1984**, *17*, 663.
- [27] J. Bastide, R. Duplessix, C. Picot, S. Candau, *Macromolecules* **1984**, *17*, 83.
- [28] M. Lang, R. Scholz, L. Löser, C. Bunk, N. Fribicz, S. Seiffert, F. Böhme, K. Saalwächter, *Macromolecules* **2022**, *55*, 5997.
- [29] I. Carmesin, K. Kremer, *Macromolecules* **1988**, *21*, 2819.
- [30] H. P. Deutsch, K. Binder, *J. Chem. Phys.* **1991**, *94*, 2294.
- [31] J. Case, *J. Polym. Sci.* **1960**, *45*, 397.
- [32] J. Scanlan, *J. Polym. Sci.* **1960**, *43*, 501.
- [33] K. Schwenke, M. Lang, J.-U. Sommer, *Macromolecules* **2011**, *44*, 9464.
- [34] M. Lang, K. Schwenke, J.-U. Sommer, *Macromolecules* **2012**, *45*, 4886.
- [35] W. Paul, K. Binder, D. W. Heermann, K. Kremer, *J. Phys. II France* **1991**, *1*, 37.
- [36] N. Clisby, *Phys. Rev. Lett.* **2010**, *104*, 055702.
- [37] J. Teixeira, *J. Appl. Cryst.* **1988**, *21*, 781.
- [38] M. Beltzung, J. Herz, C. Picot, *Macromolecules* **1983**, *16*, 580.
- [39] N. S. Davidson, R.-W. Richards, *Macromolecules* **1986**, *19*, 2576.
- [40] R. Ullman, *Macromolecules* **1982**, *15*, 1395.
- [41] D. S. Pearson, *Macromolecules* **1977**, *10*, 696.
- [42] R. Ullman, *J. Chem. Phys.* **1979**, *71*, 436.
- [43] P. J. Flory, *Polymer J.* **1985**, *17*, 1.
- [44] H. L. Trautenberg, J.-U. Sommer, D. Göritz, *J. Chem. Soc. Faraday Tran.* **1995**, *91*, 2649.
- [45] N. R. Kenkare, C. K. Hall, S. A. Khan, *J. Chem. Phys.* **2000**, *113*, 404.
- [46] J.-U. Sommer, S. Lay, *Macromolecules* **2002**, *35*, 9832.

- [47] W. Chassé, S. Schlögl, G. Riess, K. Saalwächter, *Soft Matter* **2013**, *9*, 6943.
- [48] A. Naumova, D. C. Agudelo, M. A. Villar, D. A. Vega, J. L. Valentin, K. Saalwächter, *Macromolecules* **2019**, *52*, 5042.
- [49] W. Chassé, M. Lang, J.-U. Sommer, K. Saalwächter, *Macromolecules* **2011**, *45*, 899.
- [50] M. Lang, *Macromolecules* **2017**, *50*, 2547.
- [51] T. Yamamoto, J. A. Campbell, S. Panyukov, M. Rubinstein, *Macromolecules* **2022**, *55*, 3588.
- [52] H. M. James, E. Guth, *J. Chem. Phys.* **1943**, *11*, 455.
- [53] H. M. James, E. Guth, *J. Polym. Sci.* **1949**, *4*, 153.
- [54] M. Lang, *Macromolecules* **2013**, *46*, 9782.
- [55] The discussion of the data Figure 4 in Ref. [28] contains an obvious mistake: since *square* displacements are discussed, these must be compared with the scaling of the *square* tube diameter  $\propto (\phi_0 Q)^{1/3}$ . Thus, the observed  $\beta$  is in between the expected limits set by chain expansion,  $\beta = (2\nu - 1)/(3\nu - 1) \approx 0.23$  and swelling of tube diameter,  $\beta = 1/3$ .
- [56] M. Daoud, J. P. Cotton, B. Farnoux, G. Jannink, G. Sarma, H. Benoit, R. Duplessix, C. Picot, P. G. De Gennes, *Macromolecules* **1975**, *8*, 804.
- [57] K. Saalwächter, *Prog. Nucl. Magn. Reson. Spectrosc.* **2007**, *51*, 1.